scientific data

Check for updates

OPEN

DATA DESCRIPTOR

Non-coding RNA profiling in BRAF^{V600E}-mutant cutaneous melanoma before and after Spry1 depletion

Jessica Lamberti[1,5], Domenico Memoli[1,5], Barbara Montico[2,5], Francesco Silvestro[1], Roberto Guerrieri[2], Francesca Colizzi[2], Alessandro Weisz[1,3,4], Annamaria Salvati[1]✉, Elisabetta Fratta[2]✉ & Giovanni Nassa[1,3,4]✉

Cutaneous melanoma (CM), with a continuously rising incidence worldwide, represents the most aggressive type of skin cancer, and it leads to the majority of skin cancer-related deaths. Approximately 50% of CM carry the activating BRAF^{V600} mutation and, although BRAF inhibitors have demonstrated clinical efficacy, most patients often develop early resistance to treatment. Aberrant expression of non-coding RNAs (ncRNAs), which represent less than 2% of the entire transcriptome, has been implicated in CM development and progression. By using BRAF^{V600}-mutant CM *in vitro* and *in vivo* models, we have recently demonstrated that the loss of Spry1 expression impairs BRAF^{V600}-mutant CM progression. Therefore, the extensive long and small ncRNA datasets generated in this study might represent a valuable resource for the characterization of their roles in BRAF^{V600}-mutant CM initiation and progression upon Spry1 loss, thus providing a comprehensive resource to support future studies on BRAF^{V600}-mutant CM.

Background & Summary

Cutaneous melanoma (CM) is a growing public health challenge due to its aggressive nature, rising incidence, and high mortality rates. Despite making up only 4% of all skin cancer cases, CM is responsible for nearly 75% of skin cancer-related deaths worldwide, pointing out its severity and the crucial need for improved detection and treatment strategies[1]. Early-stage localized CM is usually, successfully, treated with surgery[2], significantly increasing five-year survival rate[3]. However, a significant number of cases are diagnosed during a metastatic-advanced stage, when CM has already spread to nearby lymph nodes or other anatomic regions, resulting in frequent unresponsiveness to conventional chemotherapy and leading to a decrease of overall five-year survival to less than 10%[4].

Approximately 50% of CM patients harbor activating mutation in codon 600 of the B-Raf Proto-Oncogene Serine/Threonine kinase gene (BRAF)[5]. Of these, the substitution of valine with glutamic acid variant (V600E) accounts for 70–80% of the BRAF^{V600} mutations, resulting in the constitutive activation of the mitogen-activated protein kinase (MAPK) pathway, a key driver of CM pathogenesis[6]. As a result, FDA-approved small molecule inhibitors targeting BRAF (BRAFi) or its downstream effector MEK (MEKi), either alone or in combination, have significantly improved progression-free and overall survival of patients affected by BRAF^{V600}-mutant CM[7–9]. However, intrinsic or acquired resistance to BRAFi/MEKi poses a significant therapeutic challenge, since CM patients frequently do not respond or rapidly develop resistance to this pharmacological regimen[10,11], highlighting the urgent need of improved diagnostic and therapeutic strategies.

[1]Laboratory of Molecular Medicine and Genomics, Department of Medicine, Surgery and Dentistry 'Scuola Medica Salernitana', University of Salerno, Baronissi, (SA), Italy. [2]Immunopathology and Cancer Biomarkers Unit, Centro di Riferimento Oncologico di Aviano (CRO), IRCCS, Aviano, Italy. [3]Molecular Pathology and Medical Genomics Unit, AOU "S. Giovanni di Dio e Ruggi d'Aragona", University of Salerno, Salerno, Italy. [4]Genome Research Center for Health, Campus of Medicine, University of Salerno, Baronissi, (SA), Italy. [5]These authors contributed equally: Jessica Lamberti, Domenico Memoli, Barbara Montico. ✉e-mail: asalvati@unisa.it; efratta@cro.it; gnassa@unisa.it

In the attempt to provide novel insight into the molecular mechanisms involved in CM responsiveness to targeted therapies, we have recently identified the protein Sprouty RTK Signaling Antagonist 1 (Spry1) as a potential oncogene in $BRAF^{V600E}$-mutant metastatic CM. In fact, by using *in vitro* and *in vivo* models, we have demonstrated that Spry1 knock-out ($Spry1^{KO}$) reduced cell proliferation, causing cell cycle arrest and apoptosis, and enhanced the response to the BRAFi vemurafenib or the MEKi trametininb[12]. More recently, we have unveiled that Spry1 was mainly localized in mitochondria and that its depletion induced a metabolic rewiring by disrupting mitochondrial homeostasis and impairing glycolytic metabolism in BRAF-mutant CM cells, observing a substantial impairment of angiogenesis following $Spry1^{KO}$ [13], thus suggesting that Spry1 might be exploited as a potential target to improve $BRAF^{V600}$-mutant CM treatment.

Non-coding RNAs (ncRNAs), which account for 98% of the human genome, represent a class of RNAs without predominant protein coding function. In recent years, ncRNAs have been identified to play a pivotal role in cancer biology and treatment response, emerging as promising diagnostic and prognostic biomarkers in various types of cancer[14,15], including CM[16,17]. These molecules include a broad class of endogenous RNA transcripts such as long non-coding RNAs, linear (in this context, conventionally referred to as lncRNAs) and circular RNAs (circRNAs), as well as small non-coding RNA (sncRNAs), as microRNAs (miRNAs), piwi-interacting RNAs (piRNAs), transfer RNAs (tRNAs), small interfering RNAs (siRNAs), small nuclear RNAs (snRNAs) and small nucleolar RNAs (snoRNAs)[18].

LncRNAs are characterized by a linear structure, with transcript lengths equal or greater than 200 nucleotides, while circRNAs have a closed-loop structure, lacking both 3′ and 5′ ends. Both molecules play crucial roles as competitive endogenous RNAs (ceRNAs), accounting for an additional layer of post-transcriptional regulation[19]. LncRNAs regulate gene expression at epigenetic, transcriptional, and post-transcriptional levels. They can act as "molecular sponges" by competing with miRNAs, DNA, or transcription factors, modulating the deregulation of target proteins. In the nuclear compartment, lncRNAs can recruit or block the binding of transcription factors, directly affecting transcriptional programs. Additionally, they interact with splicing machinery or nascent RNAs, guiding specific splicing patterns[20]. In the cytoplasm, lncRNAs have proven to impact on gene expression mainly at post-transcriptional level by regulating the polysome loading on messenger RNAs (mRNAs), by controlling internal ribosomal entry sites, or by facilitating mRNA decay[21]. On the other hand, circRNAs can also act as miRNA sponges to regulate gene expression by controlling alternative splicing, transcription, and protein translation, as well as by influencing the ceRNA mechanism[22].

Both lncRNAs and circRNAs have raised increasing interest in CM biology due to their roles in influencing tumor growth, invasion, and resistance to targeted therapies[17]. Given their aberrant expression in CM, they might serve as promising biomarkers and therapeutic vulnerabilities to be targeted by RNA interference (RNAi), antisense oligonucleotides (ASOs) and CRISPR/Cas9-based genome editing [17]. On the other hand, miRNAs represent the most studied sncRNAs in CM as these molecules of approximately 21–23 nt in length play a crucial role in gene regulation by controlling the expression of complementary target mRNAs at the post-transcriptional level, either by repressing translation or promoting their degradation[23]. Considering their tumor-enhancing or -inhibiting properties, miRNAs are classified as oncomiRs or tumor-suppressor miRNAs[24], and an imbalance of their expression levels has been shown to influence the major molecular events that occur during CM development and progression, including cell proliferation, invasion, metastasis, and resistance to MAPK inhibitors[25–27]. As a result, an increasing amount of studies have investigated the predictive and prognostic potential of specific miRNA signatures in CM[28,29]. Additionally, miRNAs have also emerged as potential non-invasive diagnostic molecules due to their ability to be released into biological fluids[30], where they exhibit notable stability and are easily detectable through liquid biopsy[31,32].

Considering these premises, the present study aims to provide a useful resource for the characterization of lnc-, circ-, and snc-RNAs in $BRAF^{V600E}$-mutant metastatic CM. A schematic representation of the study design and workflow is presented in Fig. 1a.

It is worth noting that despite the availability of studies highlighting the impact of single ncRNA in CM has already been published, our work is the first to broadly encompasses the wide spectrum of expressed lnc- and sncRNAs in $BRAF^{V600E}$-mutant CM, proposing newly generated dataset from *in vitro* Mel 593 $BRAF^{V600E}$-mutant cells. LncRNAs and circRNAs datasets were extracted and annotated and validated by using our already available RNA sequencing (RNA-seq) data[12,13]. Then, for sncRNA expression profiles, we newly sequenced the small RNA fractions isolated from Mel 593, Mel 599, and Mel 611 $BRAF^{V600E}$-mutant cells, to characterize all major known sncRNA classes, including miRNAs, piRNAs, snoRNAs, snRNAs, tRNAs and rRNAs.

The analysis of the above-mentioned parental cell lines identified lncRNAs, circRNAs, and sncRNAs commonly expressed (Supplementary Table 1), along with patient-specific ncRNAs.

Evidence suggests that Spry1 may influence the expression of non-coding RNAs indirectly through its role in modulating key signaling pathways, such as MAPK, in $BRAF^{V600}$-mutant CM cells[12,33,34], exerting a regulatory control over gene expression beyond coding transcripts.

To corroborate the specificity of our data, the profile of lncRNAs and circRNAs expressed in xenografts tumors established by the subcutaneous inoculation of the BRAF-mutant Mel 272 parental and $Spry1^{KO}$ cells into athymic nude mice was analyzed according to the analytical steps detailed in the methods section. This additional new dataset may contribute to the identification of ncRNA signatures useful for the stratification of $BRAF^{V600E}$ -mutant metastatic CM patients, supporting their reuse in investigations aimed at elucidating ncRNAs involved in the CM pathogenesis and response to BRAFi.

As shown in Table 1, a total number of 5172 and 5064 distinct sncRNAs, and 29224 and 29115 lncRNAs, were detected in $BRAF^{V600E}$ -mutant parental and $Spry1^{KO}$ CM cells, respectively. The abundance of detected lncRNAs, circRNAs (Fig. 1b), and sncRNA subtypes (Fig. 1c) for each sample was detailed in Table 1. The expression patterns of previously unannotated sequences (novel-miRNAs) were also predicted as a resource for future investigations (Fig. 1c, Supplementary Table 2). Moreover, the chromosomal position of lncRNAs, circRNAs,

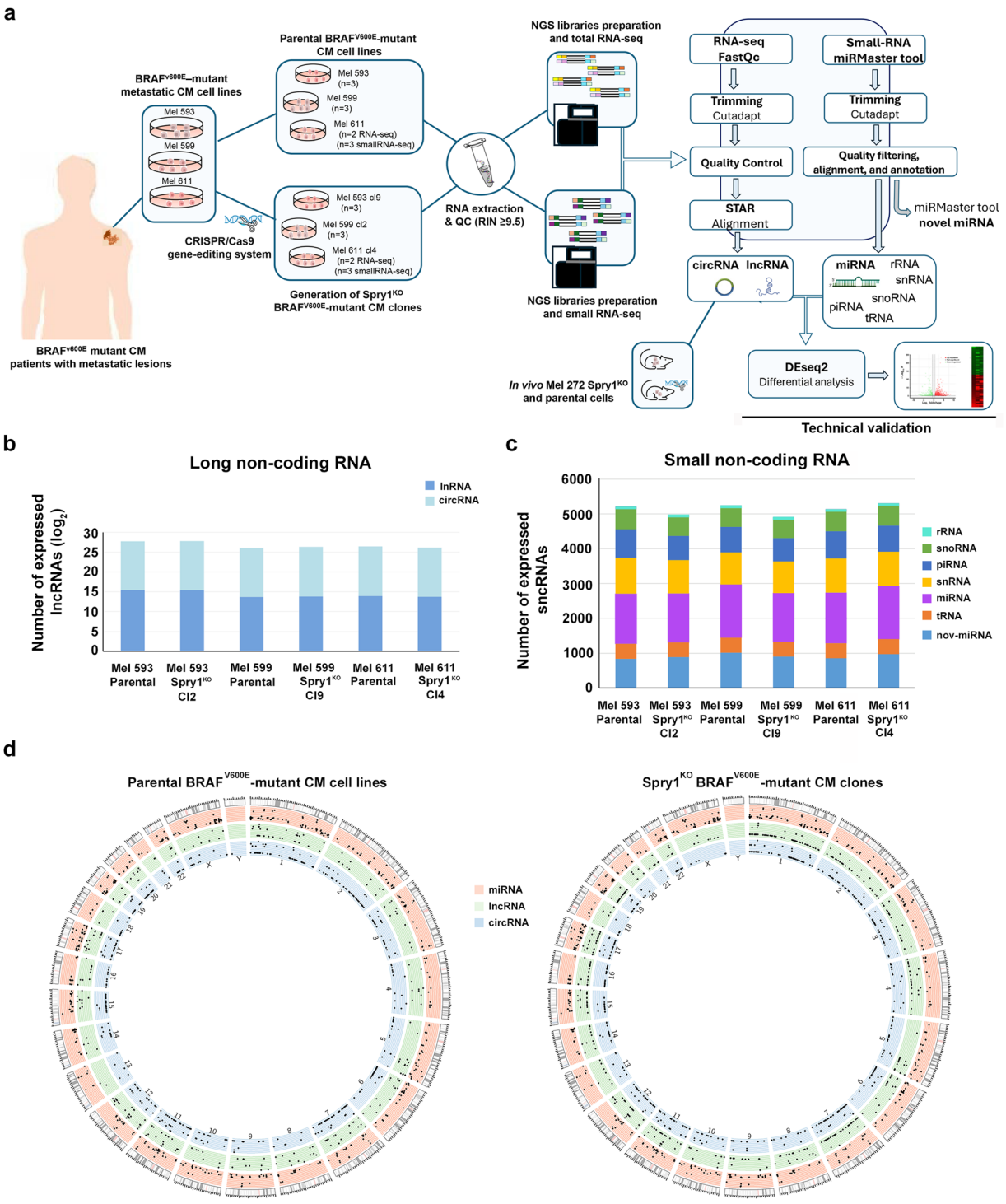

Fig. 1 Characterization of lncRNAs, circRNAs, and sncRNAsexpression profiles in BRAF^{V600E}-mutant CM cells and their Spry^{KO} clones. (**a**) Schematic representation of the experimental workflow followed to generate and validate the sncRNA datasets, including cross-analysis with lncRNAs and circRNAs from both *in vitro* and *in vivo* total RNA-seq experiments. (**b**) Bar plot showing the number of expressed lncRNAs and circRNAs in the indicated cell lines. Log_2-transformed values represent the average of replicates. (**c**) Bar plot showing the number of expressed miRNAs, novel miRNAs (nov-miRNAs), piRNAs, snRNAs, snoRNAs, and tRNAs in the indicated cell lines. Values represent an average of three replicates. (**d**) Circos plot showing genomic distribution of the first 1000 circRNAs, lncRNAs, and miRNAs detected (reads ≥ 10 for lncRNAs and circRNAs, reads ≥ 3 for miRNAs) in parental cell lines (left) and Spry1^{KO} clones (right).

Sample Name	sncRNAs	lncRNAs
Parental BRAF-V600E mutant CM cell lines	5172	29224
Spry1^{KO} BRAF-V600E mutant CM clones	5064	29115

	sncRNAs							lncRNAs	
Sample Name	miRNA	piRNA	rRNA	snoRNA	snRNA	tRNA	novel mirna	lncRNA	circRNA
Mel_593_Spry1^{KO}_cl2_rep1	1489	725	71	588	997	425	992	41500	5802
Mel_593_Spry1^{KO}_cl2_rep2	1349	666	70	506	958	419	812	42735	5431
Mel_593_Spry1^{KO}_cl2_rep3	1369	687	70	527	924	422	864	43508	4948
Mel_593_parental_rep1	1432	1016	76	615	1202	431	848	42514	5463
Mel_593_parental_rep2	1402	714	71	580	989	432	789	43557	4928
Mel_593_parental_rep3	1465	711	73	545	920	434	885	42626	5319
Mel_599_Spry1^{KO}_cl9_rep1	1363	669	72	542	836	425	897	13581	5596
Mel_599_Spry1^{KO}_cl9_rep2	1366	658	72	515	1011	424	855	14705	5885
Mel_599_Spry1^{KO}_cl9_rep3	1439	686	71	548	881	434	967	15109	5969
Mel_599_parental_rep1	1417	664	71	528	835	433	916	12689	4955
Mel_599_parental_rep2	1576	751	73	567	939	432	1053	13372	5120
Mel_599_parental_rep3	1569	782	74	547	992	433	1084	13385	5166
Mel_611_Spry1^{KO}_cl4_rep1	1595	815	72	630	1081	433	1080	15577	5965
Mel_611_Spry1^{KO}_cl4_rep2	1499	684	72	548	953	430	905	11711	4922
Mel_611_Spry1^{KO}_cl4_rep3	1472	750	72	538	914	431	944	NA	NA
Mel_611_parental_rep1	1402	725	73	526	899	429	846	15291	5803
Mel_611_parental_rep2	1417	757	71	565	950	430	835	15634	5886
Mel_611_parental_rep3	1485	803	74	568	1010	434	879	NA	NA

Table 1. Number of expressed ncRNAs.

	miRNA >= 3		circRNA >= 10		LncRNA >= 10	
Chromosome	Parental	Spry1^{KO}	Parental	Spry1^{KO}	Parental	Spry1^{KO}
Chr1	80	83	2465	2445	5350	5015
Chr2	46	45	1385	1535	3920	3960
Chr3	34	34	1430	1595	3155	3200
Chr4	22	20	905	890	1830	1490
Chr5	33	35	925	925	2550	2445
Chr6	26	26	1225	1210	2095	2435
Chr7	35	36	1030	1195	2545	2605
Chr8	22	23	510	515	2040	2080
Chr9	42	44	995	1045	1880	1760
Chr10	25	26	815	845	1850	1645
Chr11	37	38	1210	1245	2875	2775
Chr12	27	26	1125	1140	2985	2730
Chr13	17	17	360	385	1075	1035
Chr14	27	31	525	575	1800	1820
Chr15	27	26	895	955	2345	2215
Chr16	22	23	1150	1085	2470	2245
Chr17	50	51	1015	1016	3555	3275
Chr18	5	5	290	300	935	915
Chr19	39	40	1435	1480	2730	2385
Chr20	13	12	585	575	1020	995
Chr21	7	8	130	145	550	570
Chr22	27	26	510	515	1325	1255
ChrX	83	84	560	590	1270	1195
ChrY	0	0	10	10	20	45

Table 2. Genomic position of miRNAs (reads $\geq$ 3), lncRNAs and circRNAs (reads $\geq$ 10) detected.

Sample name (cell line)	Model	Protocol 1	Protocol 2	Methods	Data
Mel 593 parental_1	*In vitro*	RNA extracts (Trizol reagent)	Illumina TruSeq Stranded Total RNA Kit	—	ArrayExpress: E-MTAB-15186
Mel 593 parental_2	*In vitro*	RNA extracts (Trizol reagent)	Illumina TruSeq Stranded Total RNA Kit	—	ArrayExpress: E-MTAB-15186
Mel 593 parental_3	*In vitro*	RNA extracts (Trizol reagent)	Illumina TruSeq Stranded Total RNA Kit	—	ArrayExpress: E-MTAB-15186
Mel 593 Spry1^{KO} cl2_1	*In vitro*	RNA extracts (Trizol reagent)	Illumina TruSeq Stranded Total RNA Kit	CRISPR/Cas9 gene-editing system	ArrayExpress: E-MTAB-15186
Mel 593 Spry1^{KO} cl2_2	*In vitro*	RNA extracts (Trizol reagent)	Illumina TruSeq Stranded Total RNA Kit	CRISPR/Cas9 gene-editing system	ArrayExpress: E-MTAB-15186
Mel 593 Spry1^{KO} cl2_3	*In vitro*	RNA extracts (Trizol reagent)	Illumina TruSeq Stranded Total RNA Kit	CRISPR/Cas9 gene-editing system	ArrayExpress: E-MTAB-15186
Mel 599 parental_1	*In vitro*	RNA extracts (Trizol reagent)	Illumina TruSeq Small RNA Sample Preparation Kit	—	ArrayExpress: E-MTAB-15185
Mel 599 parental_2	*In vitro*	RNA extracts (Trizol reagent)	Illumina TruSeq Small RNA Sample Preparation Kit	—	ArrayExpress: E-MTAB-15185
Mel 599 parental_3	*In vitro*	RNA extracts (Trizol reagent)	Illumina TruSeq Small RNA Sample Preparation Kit	—	ArrayExpress: E-MTAB-15185
Mel 599 Spry1^{KO} cl9_1	*In vitro*	RNA extracts (Trizol reagent)	Illumina TruSeq Small RNA Sample Preparation Kit	CRISPR/Cas9 gene-editing system	ArrayExpress: E-MTAB-15185
Mel 599 Spry1^{KO} cl9_2	*In vitro*	RNA extracts (Trizol reagent)	Illumina TruSeq Small RNA Sample Preparation Kit	CRISPR/Cas9 gene-editing system	ArrayExpress: E-MTAB-15185
Mel 599 Spry1^{KO} cl9_3	*In vitro*	RNA extracts (Trizol reagent)	Illumina TruSeq Small RNA Sample Preparation Kit	CRISPR/Cas9 gene-editing system	ArrayExpress: E-MTAB-15185
Mel 611 parental_1	*In vitro*	RNA extracts (Trizol reagent)	Illumina TruSeq Small RNA Sample Preparation Kit	—	ArrayExpress: E-MTAB-15185
Mel 611 parental_2	*In vitro*	RNA extracts (Trizol reagent)	Illumina TruSeq Small RNA Sample Preparation Kit	—	ArrayExpress: E-MTAB-15185
Mel 611 parental_3	*In vitro*	RNA extracts (Trizol reagent)	Illumina TruSeq Small RNA Sample Preparation Kit	—	ArrayExpress: E-MTAB-15185
Mel 611 Spry1^{KO} cl4_1	*In vitro*	RNA extracts (Trizol reagent)	Illumina TruSeq Small RNA Sample Preparation Kit	CRISPR/Cas9 gene-editing system	ArrayExpress: E-MTAB-15185
Mel 611 Spry1^{KO} cl4_2	*In vitro*	RNA extracts (Trizol reagent)	Illumina TruSeq Small RNA Sample Preparation Kit	CRISPR/Cas9 gene-editing system	ArrayExpress: E-MTAB-15185
Mel 611 Spry1^{KO} cl4_3	*In vitro*	RNA extracts (Trizol reagent)	Illumina TruSeq Small RNA Sample Preparation Kit	CRISPR/Cas9 gene-editing system	ArrayExpress: E-MTAB-15185
Mel 593 parental_1	*In vitro*	RNA extracts (Trizol reagent)	Illumina TruSeq Small RNA Sample Preparation Kit	—	ArrayExpress: E-MTAB-15185
Mel 593 parental_2	*In vitro*	RNA extracts (Trizol reagent)	Illumina TruSeq Small RNA Sample Preparation Kit	—	ArrayExpress: E-MTAB-15185
Mel 593 parental_3	*In vitro*	RNA extracts (Trizol reagent)	Illumina TruSeq Small RNA Sample Preparation Kit	—	ArrayExpress: E-MTAB-15185
Mel 593 Spry1^{KO} cl9_1	*In vitro*	RNA extracts (Trizol reagent)	Illumina TruSeq Small RNA Sample Preparation Kit	CRISPR/Cas9 gene-editing system	ArrayExpress: E-MTAB-15185
Mel 593 Spry1^{KO} cl9_2	*In vitro*	RNA extracts (Trizol reagent)	Illumina TruSeq Small RNA Sample Preparation Kit	CRISPR/Cas9 gene-editing system	ArrayExpress: E-MTAB-15185
Mel 593 Spry1^{KO} cl9_3	*In vitro*	RNA extracts (Trizol reagent)	Illumina TruSeq Small RNA Sample Preparation Kit	CRISPR/Cas9 gene-editing system	ArrayExpress: E-MTAB-15185
Mel 272 parental_1	Xenograft models	RNA extracts (Trizol reagent)	Illumina TruSeq Stranded Total RNA Kit	—	ArrayExpress: E-MTAB-15369
Mel 272 parental_2	Xenograft models	RNA extracts (Trizol reagent)	Illumina TruSeq Stranded Total RNA Kit	—	ArrayExpress: E-MTAB-15369
Mel 272 parental_3	Xenograft models	RNA extracts (Trizol reagent)	Illumina TruSeq Stranded Total RNA Kit	—	ArrayExpress: E-MTAB-15369
Mel 272 Spry1^{KO} cl4_1	Xenograft models	RNA extracts (Trizol reagent)	Illumina TruSeq Stranded Total RNA Kit	CRISPR/Cas9 gene-editing system	ArrayExpress: E-MTAB-15369
Mel 272 Spry1^{KO} cl4_2	Xenograft models	RNA extracts (Trizol reagent)	Illumina TruSeq Stranded Total RNA Kit	CRISPR/Cas9 gene-editing system	ArrayExpress: E-MTAB-15369
Mel 272 Spry1^{KO} cl4_3	Xenograft models	RNA extracts (Trizol reagent)	Illumina TruSeq Stranded Total RNA Kit	CRISPR/Cas9 gene-editing system	ArrayExpress: E-MTAB-15369

Table 3. Summary of the protocols and datasets used.

and miRNAs were investigated in parental and Spry1^{KO}cells (Fig. 1d, Table 2). ncRNA transcripts were found to be expressed on almost all chromosomes in both conditions, except for chromosomes Y. Globally, regions of high miRNA expression were identified on chromosomes X and 1, whereas lncRNA and circRNA genomic positions were found enriched on chromosomes 1,2, and 3 (Table 2).

Methods

Cell lines and generation of Spry1^{KO} BRAF^{V600E}-mutant CM clones. Mel 593, Mel 599, and Mel 611 cell lines were established from metastatic lesions of BRAF^{V600E}-mutant CM patients referred to the National Cancer Institute of Aviano (Italy)[35]. Spry1^{KO} was performed using the CRISPR/Cas9 gene-editing system, as previously described by Montico and colleagues[12]. Parental and Spry1^{KO} cell lines were routinely grown in

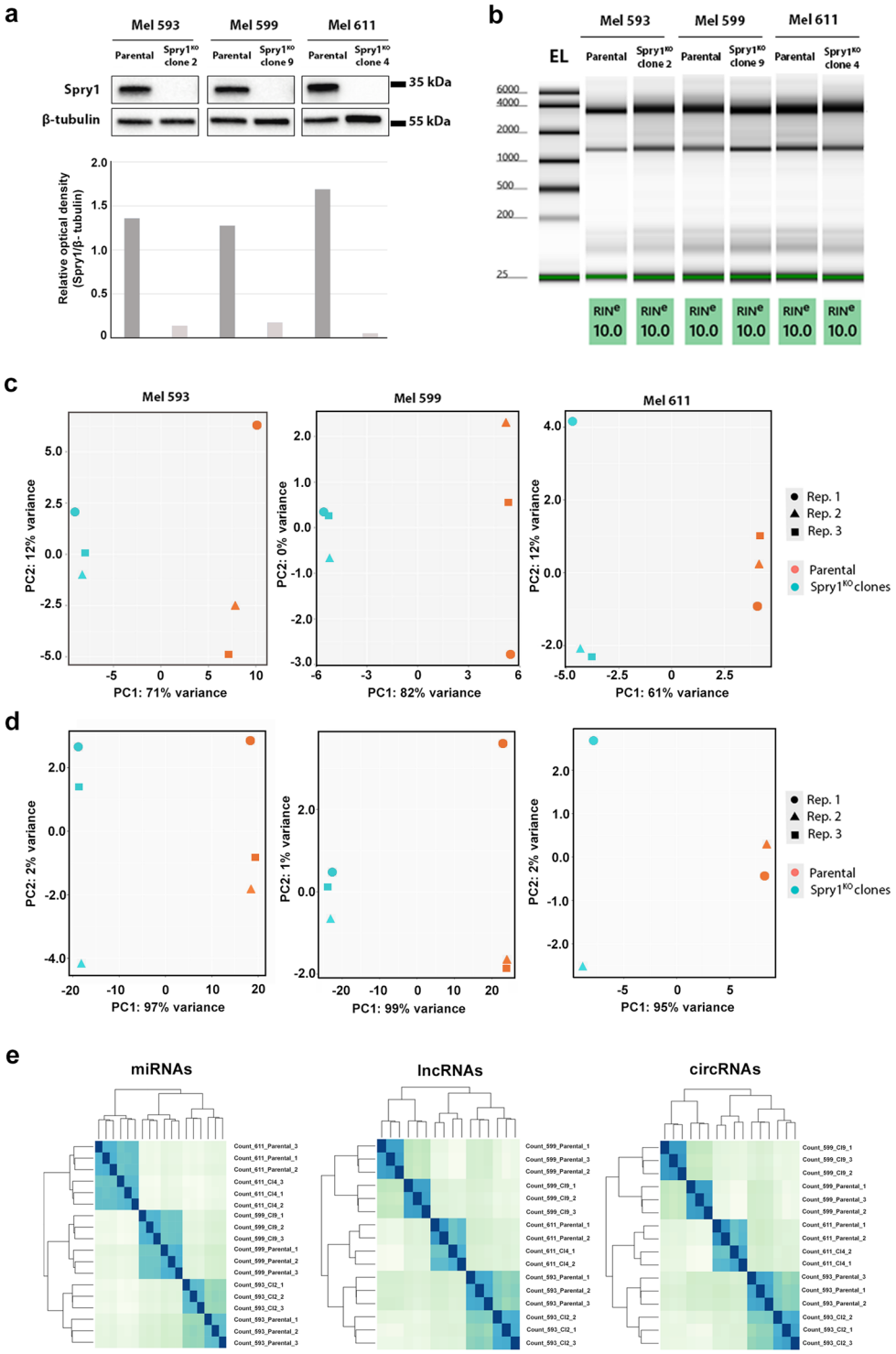

Fig. 2 Validations of the experimental procedure. (**a**) Representative western blot and relative densitometry analysis of Spry1 protein expression in parental BRAF^{V600E}-mutant CM cell lines and their respective Spry1^{KO} clones. β-tubulin was used as a loading control. Images were processed with ImageJ software (https://imagej.Net) for densitometry readings. (**b**) Gel-like images of tape station analysis of total RNA samples from parental and Spry1^{KO} cell lines, showing RIN values. One representative replicate of three is shown for each cell line. EL indicates the electronic ladder. PCA of sncRNAs (**c**) and ncRNAs (**d**) in parental and Spry1^{KO} cells. Different shapes (circles, triangles, and squares) indicate biological/technical replicates, color-coded according to cell lines. The first two components (PC1 and PC2) are shown. (**e**) Correlation heatmaps of miRNAs (left), lncRNAs (middle), and circRNAs (right) expression across the samples.

Sample Name	Nanodrop		RIN
	260/280	260/230	
Mel_593_Spry1^{KO}_cl2_rep1	2.0	2.1	9.5
Mel_593_Spry1^{KO}_cl2_rep2	2.0	2.1	10.0
Mel_593_Spry1^{KO}_cl2_rep3	2.0	2.1	10.0
Mel_593_parental_rep1	2.0	2.0	10.0
Mel_593_parental_rep2	2.0	2.1	10.0
Mel_593_parental_rep3	2.0	2.0	10.0
Mel_599_Spry1^{KO}_cl9_rep1	2.0	2.0	10.0
Mel_599_Spry1^{KO}_cl9_rep2	2.0	1.9	10.0
Mel_599_Spry1^{KO}_cl9_rep3	2.0	2.2	10.0
Mel_599_parental_rep1	2.0	2.1	9.9
Mel_599_parental_rep2	2.0	2.2	10.0
Mel_599_parental_rep3	2.0	2.2	10.0
Mel_611_Spry1^{KO}_cl4_rep1	2.0	2.1	10.0
Mel_611_Spry1^{KO}_cl4_rep2	2.0	1.9	10.0
Mel_611_Spry1^{KO}_cl4_rep3	2.0	2.1	9.9
Mel_611_parental_rep1	2.0	2.1	10.0
Mel_611_parental_rep2	2.0	2.1	10.0
Mel_611_parental_rep3	2.0	2.1	10.0

Table 4. RNA quality controls.

Sample Name	Total reads	GC Content (%)	Mean Phred Score	Mean Read Length (nt)	% alignment on Human genome
Mel_593_Spry1^{KO}_cl2_rep1	21113751	49.26	35	23	91.18
Mel_593_Spry1^{KO}_cl2_rep2	20221274	47.63	35	23	93.69
Mel_593_Spry1^{KO}_cl2_rep3	26114908	47.87	35	23	93.36
Mel_593_parental_rep1	24364885	49.64	35	23	94.31
Mel_593_parental_rep2	16482033	48.78	35	23	92.87
Mel_593_parental_rep3	21146212	48.04	35	23	92.97
Mel_599_Spry1^{KO}_cl9_rep1	15038881	47.05	35	23	90.49
Mel_599_Spry1^{KO}_cl9_rep2	13483049	48.05	35	23	92.84
Mel_599_Spry1^{KO}_cl9_rep3	21840777	47.11	35	23	87.56
Mel_599_parental_rep1	13433885	49.96	35	23	91.96
Mel_599_parental_rep2	22072527	48.29	35	23	90.31
Mel_599_parental_rep3	21333463	48.29	35	23	92.16
Mel_611_Spry1^{KO}_cl4_rep1	34156786	50.39	35	23	91.51
Mel_611_Spry1^{KO}_cl4_rep2	24677873	49.03	35	23	93.58
Mel_611_Spry1^{KO}_cl4_rep3	19566185	47.32	35	23	94.87
Mel_611_parental_rep1	19608269	47.99	35	23	94.81
Mel_611_parental_rep2	20105571	48.55	35	23	94.23
Mel_611_parental_rep3	24690632	49.12	35	23	93.84

Table 5. sncRNA sequencing quality metrics for samples.

RPMI-1640 medium, supplemented with 10% heat-inactivated fetal calf serum (FCS, Lonza), 100 μg/mL streptomycin, and 100 IU/mL penicillin. Cells were maintained in a humidified incubator at 37 °C in 5% CO2 and routinely tested for mycoplasma contamination.

***In vivo* models.** Xenograft models were established by subcutaneously injecting Mel 272 parental and Spry1^{KO} cells into six-week-old female athymic nude/nude mice, as detailed by Montico and colleagues[12]. All the preclinical studies were performed in accordance with the Internal Review Board of the Centro di Riferimento Oncologico, IRCCS-National Cancer Institute, Aviano, Italy (IRB number 07-2017) and the Italian Ministry of Health (no. 788/2015/PR).

Western blot analysis for Spry1^{KO} validation. Total protein lysate extraction and western blot were performed as previously reported[12,14]. The membranes were immunoblotted with the following primary antibodies according to their manufacturer's instructions: rabbit monoclonal anti-Spry (#13013, Cell Signaling Technologies) and mouse monoclonal anti-β Tubulin (#86298, Cell Signaling Technologies). Images were

Sample Name	Total reads	GC Content (%)	Mean Phred Score	Mean Read Length (nt)
Mel_593_Spry1KO_cl2_rep1	56105232	45	34	20-76
Mel_593_Spry1KO_cl2_rep2	52468092	45	34	20-76
Mel_593_Spry1KO_cl2_rep3	49220380	44	34	20-76
Mel_593_parental_rep1	40794696	45	33	20-76
Mel_593_parental_rep2	49570314	44	34	20-76
Mel_593_parental_rep3	51224950	45	34	20-76
Mel_599_Spry1KO_cl9_rep1	83231150	46	36	20-76
Mel_599_Spry1KO_cl9_rep2	94202792	46	36	20-76
Mel_599_Spry1KO_cl9_rep3	95235566	46	36	20-76
Mel_599_parental_rep1	59902188	45	36	20-76
Mel_599_parental_rep2	70398042	44	36	20-76
Mel_599_parental_rep3	70989586	44	36	20-76
Mel_611_Spry1KO_cl4_rep1	94015856	46	34	20-76
Mel_611_Spry1KO_cl4_rep2	92599778	46	34	20-76
Mel_611_parental_rep1	98914256	45	34	20-76
Mel_611_parental_rep2	93776810	46	34	20-76

Table 6. Total RNA sequencing quality metrics for samples.

captured and analyzed using the Chemidoc XRS + system (Bio-Rad). Densitometry was performed by ImageJ software analysis[36].

RNA isolation and quality controls. Total RNA for small RNA-seq experiment was extracted from Mel 593, Mel 599, and Mel 611 parental and Spry1^{KO}cells, using Trizol reagent (Invitrogen). Three biological replicates were processed for each sample, resulting in 18 samples. RNA concentration was determined with a NanoDrop ND-2000 spectrophotometer (Thermo Fisher Scientific) by evaluating the absorbance ratios A260/A280 and A230/A280. RNA integrity was assessed using the TapeStation System (Agilent Technologies, Milan, Italy).

Small RNA-seq library preparation and sequencing. For small RNA-seq, 1 μg of total RNA from each cell line was used for library preparation with the Illumina TruSeq Small RNA Sample Preparation Kit (Illumina Inc., San Diego, CA, USA), according to the manufacturer's protocol. In summary, 3′ and 5′ adapters were ligated to small RNAs in a sequential manner, followed by reverse transcription to synthesize cDNA. The samples were then amplified and indexed through 15 cycles of PCR. The resulting PCR products were purified using a 6% polyacrylamide gel, selecting fragments shorter than 200 nucleotides, and subsequently precipitated with ethanol. The experiment was performed in three independent replicates for each condition. Final library concentrations and sizes were assessed using the Quant-IT DNA Assay Kit and TapeStation System. All libraries were then equimolarly pooled, diluted to a final concentration of 1,3 pM, and sequenced as single reads (75 cycles) on the Illumina NextSeq. 500 platform (Illumina, San Diego, CA).

RNA-seq analysis. Quality control analysis of lncRNAs and circRNAs raw sequences files (fastq files), obtained from previously published RNA-seq datasets[12,13] (Mel 599 and Mel 611 clones) as well as the newly available mel 593 RNA-seq data, was performed using FastQc (v0.11.8) (http://www.bioinformatics.babraham.ac.uk/projects/fastqc/). Adapter sequences were trimmed using Cutadapt (v3.7)[37] with default parameters, setting a minimum read length of 20 bp. Filtered reads were aligned on the hg38 human genome assembly using STAR (v2.7.11b)[38] with default parameters and gene quantification was obtained with featureCount (v2.0.3)[39] to assess the expression of lncRNAs and circRNAs. The counts were then imported in R (v4.5.0) and DEseq. 2 (v1.48.1)[40] was used to identify differentially expressed transcripts, applying a threshold of fold change ($|FC| \geq 1.5$ and an adjusted p-value ≤ 0.05, to evaluate the impact of Spry1^{KO} on lncRNA and circRNA expression profiles. The chromosomal distribution of lnRNAs and circRNAs (reads ≥ 10) was mapped onto the hg38 human genome assembly, whereas Circos[41] was used to generate Circos plots. The function EnhancedVolcano (https://github.com/kevinblighe/EnhancedVolcano) was used to generate volcano plots. Heatmaps and hierarchical clustering were generated using countMatrix.

Small RNA-seq analysis. After sequencing, sncRNAfastq files were processed using the miRMaster tool (v2.0)[42] selecting the standard parameters for quality filtering, alignment, and annotation of sncRNAs. The miRMaster pipeline was configured to reference the following annotation databases: miRBase (v22.1)[43], Ensembl ncRNA (v100) (https://www.ensembl.org/), RNACentral piRNA (v15)[44], GtRNAdb (v18.1)[45], circBase (accessed on 25.10.20)[46], NCBI RefSeq for bacteria and viruses (v74)[47], and NONCODE (v5)[48]. Adapter trimming was performed with Cutadapt (v3.7) using the following small RNA adapter sequences: 3′ adapter TGGAATTCTCGGGTGCCAAGG and 5′ adapter GTTCAGAGTTCTACAGTCCGACGATC. DEseq. 2 (v1.48.1)[40] was used to perform a differential expression analysis, applying a threshold of $|FC| \geq 1.5$ and an adjusted p-value ≤ 0.05, to detect miRNAs whose expression was significantly modulated by Spry1 depletion. miRNA target prediction was performed using the miRMaster tool. Novel miRNA candidates were predicted by miRMaster through genome-wide mapping of unannotated small RNA reads, followed by secondary structure

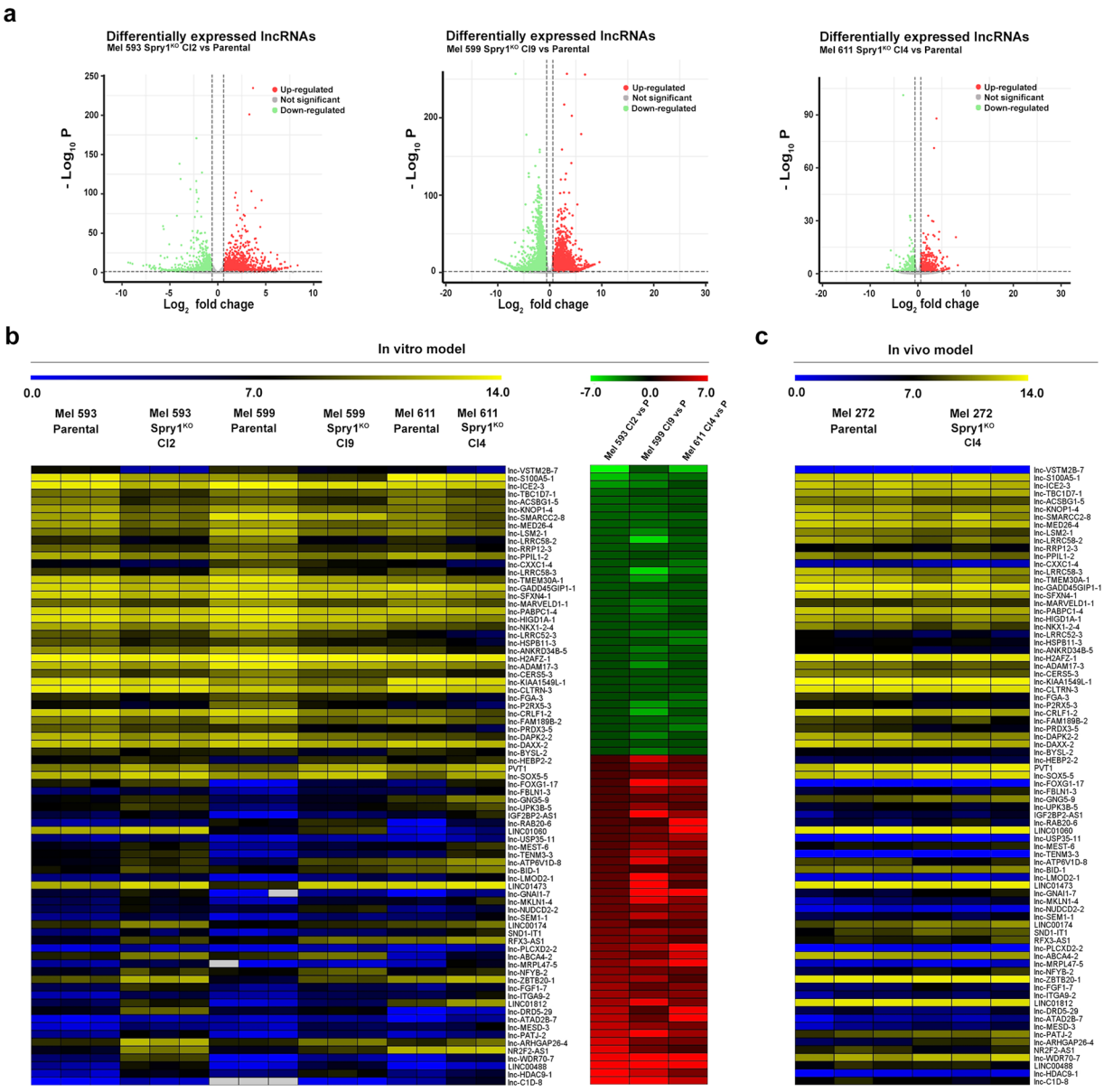

Fig. 3 Analysis of lncRNA expression profiles. (**a**) Volcano plot summarizing significantly up-regulated (red) and down-regulated (green) lncRNAs in Spry^{KO} clones; lncRNAs with insignificant expression values are reported in grey. Significance was determined based on $\log_2$ FC cutoff of ± 1.5 and adjusted p-values threshold of 0.05. (**b**) Heatmaps showing expression (left) with respect to FC (right) of common, concordantly deregulated lncRNAs ($|FC| \geq 1.5$, adjusted p-value ≤ 0.05) across Spry1^{KO} clones compared to the parental cell lines. (**c**) Heatmap showing expression of the same commonly deregulated lncRNAs in xenograft tumors derived from Mel272 parental and Spry1^{KO} cells. RNA-seq data supporting Fig. 3 are available in ArrayExpress with accession number E-MTAB-15186[49] (Mel 593 *in vitro* clones) and E-MTAB-15369[51] (Mel 272 *in vivo* clones).

prediction and evaluation of typical miRNA features such as stem-loop formation, read distribution bias, and minimum free energy criteria. The chromosomal distribution of miRNAs (reads ≥ 3) was mapped onto the hg38 human genome assembly, whereas Circos[41] was used to generate Circos plots. The function EnhancedVolcano (https://github.com/kevinblighe/EnhancedVolcano) was used to generate volcano plots. Heatmaps and hierarchical clustering were generated using countMatrix.

Data Records

Raw data generated in the study were deposited in ArrayExpress repository with E-MTAB-15186[49] (Mel 593 RNA-seq parental and Spry1^{KO} clones), E-MTAB-15185[50] for small RNA-seq (Mel 593, Mel 599, and Mel 611 parental and Spry1^{KO} cells) and E-MTAB-15369[51] (Mel 272 RNA-seq parental and Spry1^{KO} *in vivo* clones). All relevant information concerning samples, useful for their reuse, are available in Table 3.

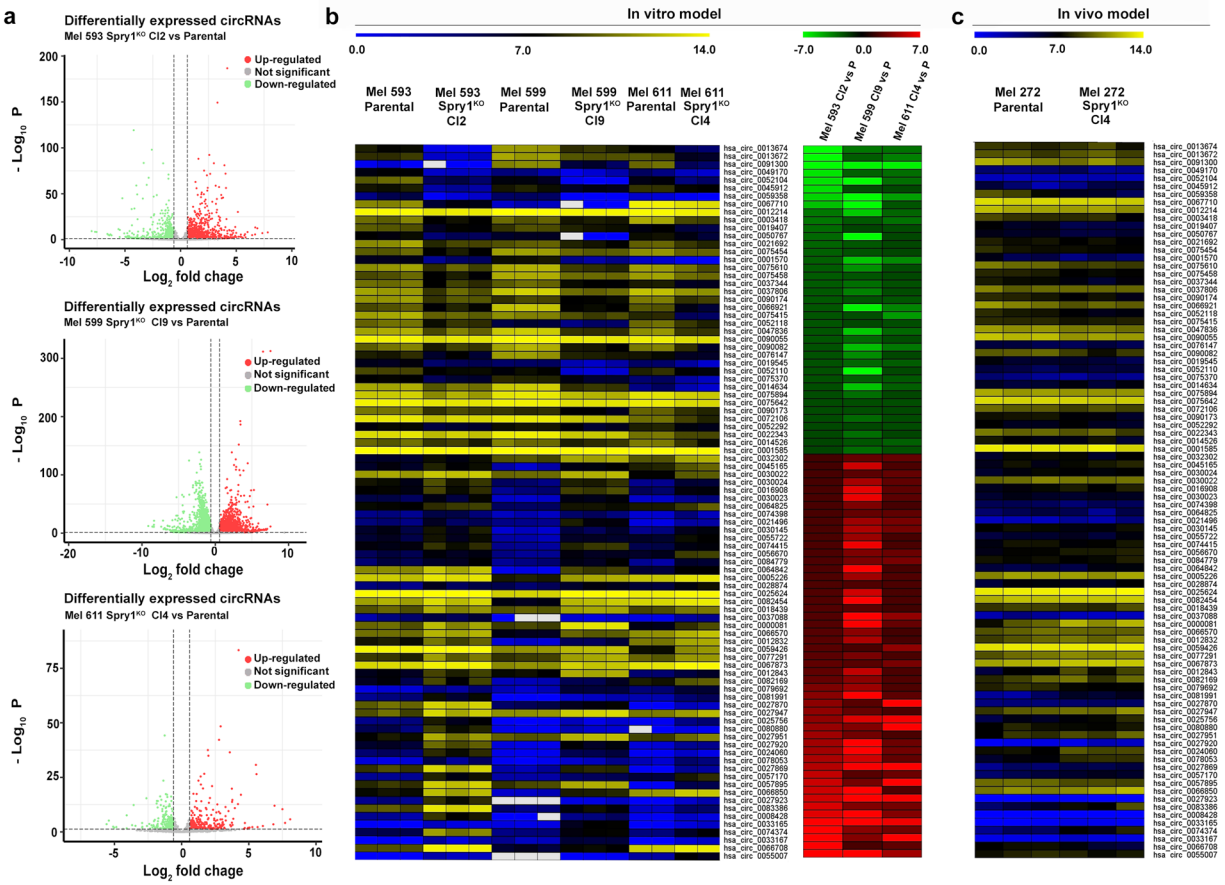

Fig. 4 Analysis of circRNA expression profiles. (**a**) Volcano plot summarizing significantly up-regulated (red) and down-regulated (green) circRNAs in Spry^{KO} clones;circRNAs with insignificant expression values are reported in grey. Significance was determined based on log2FC cutoff of ± 1.5 and adjusted p-values threshold of 0.05. (**b**) Heatmaps showing expression (left) with respect to FC (right) of common, concordantly deregulated circRNAs ($|FC| \geq 1.5$, adjusted p-value ≤ 0.05) across Spry1^{KO} clones compared to the parental cell lines. (**c**) Heatmap showing expression of the same commonly deregulated circRNAs in xenograft tumors derived from Mel272 parental and Spry1^{KO} cells. RNA-seq data supporting Fig. 4 are available in ArrayExpress with accession number E-MTAB-15186[49] (Mel 593 *in vitro* clones) and E-MTAB-15369[51] (Mel 272 *in vivo* clones).

Technical Validation

Spry1^{KO} validation. To validate the reliability and consistency of our experimental model, we have reported the western blot analysis of Spry1 depletion. As shown in Fig. 2a, Spry1 was not expressed in Spry1^{KO}cells, thus confirming the complete loss of Spry1 protein expression, and ensuring the robustness of subsequent experimental analyses.

Assessment of RNA quality. RNA purity and integrity are essential when preparing samples for RNA-seq experiments to ensure the reliability of subsequent experimental analyses. Hence, stringent quality control of RNA samples was performed before library preparation, as described in the methods section. All samples used for the small RNA-seq experiments had an RNA integrity number (RIN) ≥ 9.5, with 260/280 and 260/230 ratios between 1.9 and 2.2, indicating that the RNAs were intact and free of phenolic and protein contaminants (Fig. 2b, Table 4).

Total and Small RNA-seq summarization and quality controls. To assess the sequencing data's quality and reliability, we evaluated key sequencing parameters from both small RNA-seq (Table 5) and total RNA-seq (Table 6) experiments, including read count and base-call accuracy. The average number of raw reads per sample was 21.08 ± 4.94 million for small RNA-seq and 72.04 ± 20.8 million for total RNA-seq. Notably, the evaluation of alignment efficiency of small RNA-seq experiment revealed a mean alignment percentage to human genome of $92.58 \pm 1.86\%$. The mean GC content per sample was $48.47 \pm 0.96\%$ for small RNA-seq and $45.13 \pm 0.81\%$ for total RNA-seq, and the average read length was consistent with the expected fragment size for each sequencing approach. The mean Phred score was 35 for both small RNA-seq and total RNA-seq, indicating high base calling accuracy. Additionally, we assessed the same key sequencing parameters for *in vivo* total RNA-seq experiment (Supplementary Table 3).

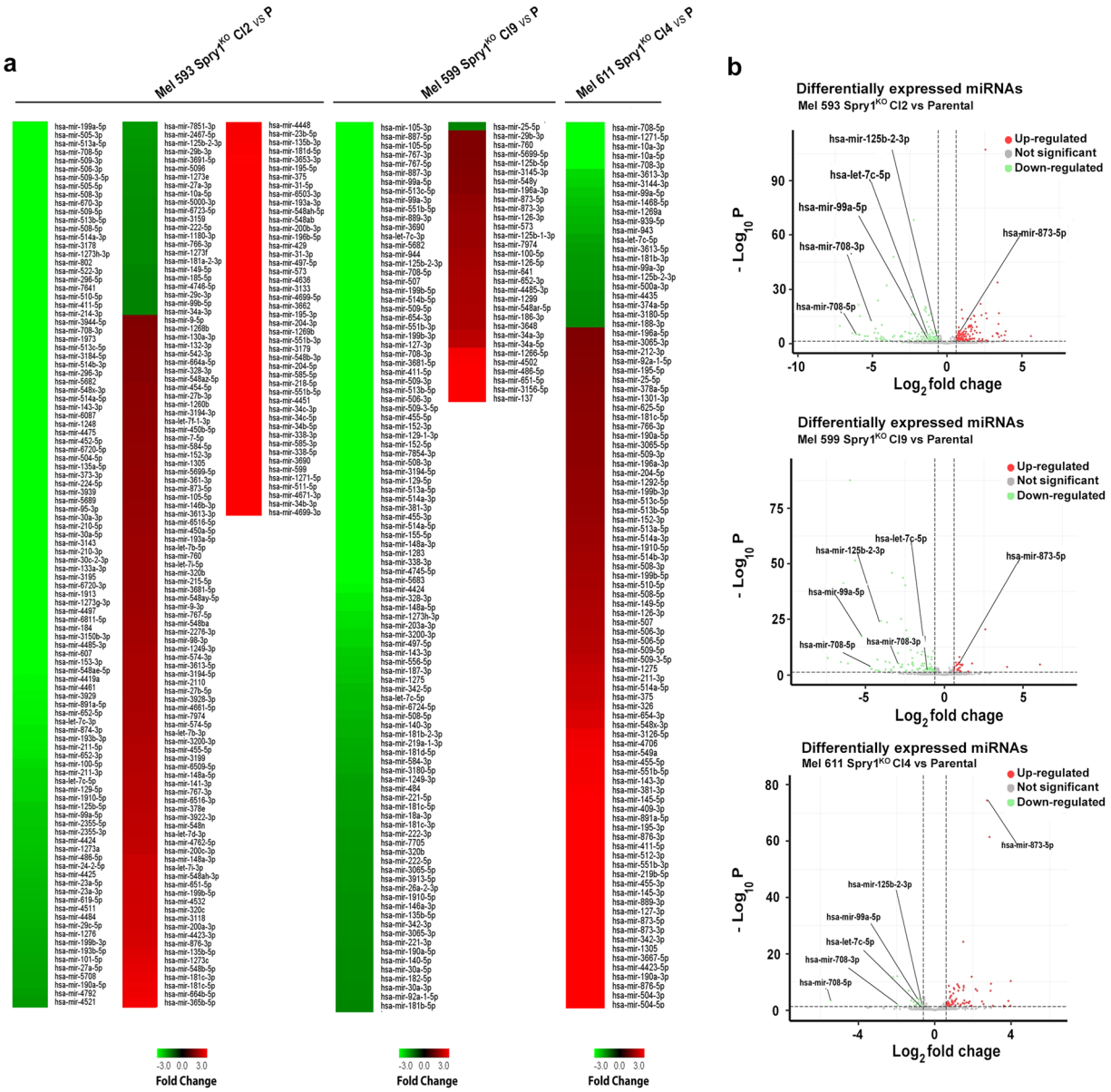

Fig. 5 Analysis of miRNA expression profiles. (**a**) Heatmaps showing up-regulated (red) and down-regulated expressed (green) miRNAs upon Spry1 depletion ($|FC| \geq 1.5$, adjusted p-value ≤ 0.05) in the indicated cell lines. (**b**) Volcano plot summarizing significantly up-regulated (red) and down-regulated (green) miRNAs in Spry^{KO} clones; miRNAs with insignificant expression values are reported in grey. Significance was determined based on log2 FC cutoff of ± 1.5 and adjusted p-values threshold of 0.05. Commonly deregulated miRNAs across the clones are highlighted in bold. Small RNA-seq data supporting Fig. 5 are available in ArrayExpress with accession number E-MTAB-15185[50] (Mel 593, Mel 599, and Mel 611 parental and Spry1^{KO} cells).

Reproducibility validation. Principal component analysis (PCA) was performed to assess the biological significance of Spry1^{KO}on sncRNA and ncRNA expression profiles and to evaluate the accuracy of library preparation and sequencing procedures. The variation along the principal component (PC) 1 axis was above 60% for sncRNAs and above 95% for ncRNAs across all three cell lines, indicating that Spry1^{KO} significantly altered both expression profiles. The variation along the PC2 was below 20% for sncRNAs and 2% for ncRNAs, validating the reproducibility of biological replicates and repeatability of technical assessments (Fig. 2c,d). Furthermore, we performed a correlation analysis on the normalized read counts of miRNAs, lncRNAs, and circRNAs across all samples. The resulting correlation heatmap showed a high intra-group correlation among biological and technical replicates for all ncRNA classes, both before and after Spry1 depletion (Fig. 2e).

ncRNAs differential expression analyses. To further validate our new datasets, lncRNAs and circRNAs derived from Mel 593 were compared to those obtained from Mel 599, and Mel 611 cell lines following Spry1^{KO} [12,13], to enable comprehensive overview of ncRNAs that might be related to Spry1 in BRAF^{V600E}-mutant CM. This revealed 3869, 9397, and 781 differentially expressed lncRNAs (Fig. 3a, Supplementary Table 4) and 1804, 3909, and

656 differentially expressed circRNAs (Fig. 4a, Supplementary Table 5) in Mel 593, Mel 599, and Mel 611, respectively. Moreover, 79 lncRNAs and 90 circRNAs were commonly deregulated across all three cell lines, validating our new datasets, as showed by their expression levels in both parental cell lines and Spry1^{KO} clones (Figs. 3b, 4b, Supplementary Tables 6, 7). Then, we newly assessed their expression in xenograft tumors derived from parental and Mel272 Spry1^{KO} Cl4 cells and observed similar dysregulation for most of them (Figs. 3c, 4c, Supplementary Tables 6, 7). The same approach was applied for miRNAs. The analysis led to the identification of 256, 130, and 96 differentially expressed miRNAs in Mel 593, Mel 599, and Mel 611, respectively (Fig. 5a,b, Supplementary Table 8). This confirmed the reliability of our RNA-seq data sustaining that the experiments were conducted appropriately and match among different methods and settings.

Received: 13 June 2025; Accepted: 13 August 2025;
Published online: 02 September 2025

References

1. Gosman, L. M., Ţăpoi, D.-A. & Costache, M. Cutaneous melanoma: A review of multifactorial pathogenesis, immunohistochemistry, and emerging biomarkers for early detection and management. *Int. J. Mol. Sci.* **24** (2023).
2. Orzan, O. A., Şandru, A. & Jecan, C. R. Controversies in the diagnosis and treatment of early cutaneous melanoma. *J. Med. Life* **8**, 132–141 (2015).
3. Savage, D. J. *et al*. Patterns in progression from early-stage melanoma to late-stage melanoma: implications for survivorship follow-up. *Melanoma Manag.* **11**, 2424708 (2024).
4. Kudchadkar, R. R., Lowe, M. C., Khan, M. K. & McBrien, S. M. Metastatic melanoma. *CA Cancer J. Clin.* **70**, 78–85 (2020).
5. Castellani, G. *et al*. BRAF mutations in melanoma: biological aspects, therapeutic implications, and circulating biomarkers. *Cancers (Basel)* **15** (2023).
6. Guo, W., Wang, H. & Li, C. Signal pathways of melanoma and targeted therapy. *Signal Transduct. Target. Ther.* **6**, 424 (2021).
7. Giugliano, F. *et al*. First line treatment of BRAF mutated advanced melanoma: Does one size fit all? *Cancer Treat. Rev.* **99**, 102253 (2021).
8. Tanda, E. T. *et al*. Current state of target treatment in BRAF mutated melanoma. *Front. Mol. Biosci.* **7**, 154 (2020).
9. Grimaldi, A. M. *et al*. MEK inhibitors in the treatment of metastatic melanoma and solid tumors. *Am. J. Clin. Dermatol.* **18**, 745–754 (2017).
10. Dulgar, O., Kutuk, T. & Eroglu, Z. Mechanisms of Resistance to BRAF-Targeted Melanoma Therapies. *Am. J. Clin. Dermatol.* **22**, 1–10 (2021).
11. Luebker, S. A. & Koepsell, S. A. Diverse mechanisms of BRAF inhibitor resistance in melanoma identified in clinical and preclinical studies. *Front. Oncol.* **9**, 268 (2019).
12. Montico, B. *et al*. Loss of Spry1 reduces growth of BRAFV600-mutant cutaneous melanoma and improves response to targeted therapy. *Cell Death Dis.* **11**, 392 (2020).
13. Montico, B. *et al*. Suppression of Spry1 reduces HIF1α-dependent glycolysis and impairs angiogenesis in BRAF-mutant cutaneous melanoma. *J. Exp. Clin. Cancer Res.* **44**, 53 (2025).
14. Zhang, X. *et al*. Non-coding RNAs' function in cancer development, diagnosis and therapy. *Biomed. Pharmacother.* **167**, 115527 (2023).
15. Eldakhakhny, B. *et al*. Exploring the role of noncoding RNAs in cancer diagnosis, prognosis, and precision medicine. *Noncoding RNA Res* **9**, 1315–1323 (2024).
16. Peng, Q. & Wang, J. Non-coding RNAs in melanoma: Biological functions and potential clinical applications. *Mol. Ther. Oncolytics* **22**, 219–231 (2021).
17. Montico, B. *et al*. The pleiotropic roles of circular and long noncoding RNAs in cutaneous melanoma. *Mol. Oncol.* **16**, 565–593 (2022).
18. Russell, S. J. *et al*. An atlas of small non-coding RNAs in human preimplantation development. *Nat. Commun.* **15**, 8634 (2024).
19. Ala, U. Competing Endogenous RNAs, Non-Coding RNAs and Diseases: An Intertwined Story. *Cells* **9** (2020).
20. Fernandes, J. C. R., Acuña, S. M., Aoki, J. I., Floeter-Winter, L. M. & Muxel, S. M. Long Non-Coding RNAs in the Regulation of Gene Expression: Physiology and Disease. *Noncoding RNA* **5** (2019).
21. Statello, L., Guo, C.-J., Chen, L.-L. & Huarte, M. Author Correction: Gene regulation by long non-coding RNAs and its biological functions. *Nat. Rev. Mol. Cell Biol.* **22**, 159 (2021).
22. Conn, V. M., Chinnaiyan, A. M. & Conn, S. J. Circular RNA in cancer. *Nat. Rev. Cancer* **24**, 597–613 (2024).
23. O'Brien, J., Hayder, H., Zayed, Y. & Peng, C. Overview of microrna biogenesis, mechanisms of actions, and circulation. *Front Endocrinol (Lausanne)* **9**, 402 (2018).
24. Otmani, K., Rouas, R., Berehab, M. & Lewalle, P. The regulatory mechanisms of oncomiRs in cancer. *Biomed. Pharmacother.* **171**, 116165 (2024).
25. Poniewierska-Baran, A. *et al*. Role of miRNA in Melanoma Development and Progression. *Int. J. Mol. Sci.* **24** (2022).
26. Gajos-Michniewicz, A. & Czyz, M. Role of miRNAs in Melanoma Metastasis. *Cancers (Basel)* **11** (2019).
27. Motti, M. L., Minopoli, M., Di Carluccio, G., Ascierto, P. A. & Carriero, M. V. Micrornas as key players in melanoma cell resistance to MAPK and immune checkpoint inhibitors. *Int. J. Mol. Sci.* **21** (2020).
28. Lu, T. *et al*. Identification of a five-miRNA signature predicting survival in cutaneous melanoma cancer patients. *PeerJ* **7**, e7831 (2019).
29. Dika, E. *et al*. Defining the prognostic role of microrna in cutaneous melanoma. *J. Invest. Dermatol.* **140**, 2260–2267 (2020).
30. Pozniak, T., Shcharbin, D. & Bryszewska, M. Circulating microRNAs in Medicine. *Int. J. Mol. Sci.* **23** (2022).
31. Sabato, C. *et al*. A novel microRNA signature for the detection of melanoma by liquid biopsy. *J. Transl. Med.* **20**, 469 (2022).
32. Van Laar, R. *et al*. Validation of a microRNA liquid biopsy assay for diagnosis and risk stratification of invasive cutaneous melanoma. *Br. J. Dermatol.* **189**, 292–301 (2023).
33. Saj, A. & Lai, E. C. Control of microRNA biogenesis and transcription by cell signaling pathways. *Curr. Opin. Genet. Dev.* **21**, 504–510 (2011).
34. Ishikawa, T. *et al*. Long Non-Coding RNAs Associated with Mitogen-Activated Protein Kinase in Human Pancreatic Cancer. *Cancers (Basel)* **15** (2023).
35. Altomonte, M. *et al*. Differential expression of cell adhesion molecules CD54/CD11a and CD58/CD2 by human melanoma cells and functional role in their interaction with cytotoxic cells. *Cancer Res.* **53**, 3343–3348 (1993).
36. Schneider, C. A., Rasband, W. S. & Eliceiri, K. W. NIH Image to ImageJ: 25 years of image analysis. *Nat. Methods* **9**, 671–675 (2012).
37. Martin, M. Cutadapt removes adapter sequences from high-throughput sequencing reads. *EMBnet j.* **17**, 10 (2011).
38. Dobin, A. *et al*. STAR: ultrafast universal RNA-seq aligner. *Bioinformatics* **29**, 15–21 (2013).
39. Liao, Y., Smyth, G. K. & Shi, W. The R package Rsubread is easier, faster, cheaper and better for alignment and quantification of RNA sequencing reads. *Nucleic Acids Res.* **47**, e47 (2019).

40. Love, M. I., Huber, W. & Anders, S. Moderated estimation of fold change and dispersion for RNA-seq data with DESeq. 2. *Genome Biol.* **15**, 550 (2014).
41. Krzywinski, M. *et al*. Circos: an information aesthetic for comparative genomics. *Genome Res.* **19**, 1639–1645 (2009).
42. Fehlmann, T. *et al*. miRMaster 2.0: multi-species non-coding RNA sequencing analyses at scale. *Nucleic Acids Res.* **49**, W397–W408 (2021).
43. Kozomara, A., Birgaoanu, M. & Griffiths-Jones, S. miRBase: from microRNA sequences to function. *Nucleic Acids Res.* **47**, D155–D162 (2019).
44. The RNAcentral Consortium. RNAcentral: a hub of information for non-coding RNA sequences. *Nucleic Acids Res.* **47**, D221–D229 (2019).
45. Chan, P. P. & Lowe, T. M. GtRNAdb 2.0: an expanded database of transfer RNA genes identified in complete and draft genomes. *Nucleic Acids Res.* **44**, D184–9 (2016).
46. Glažar, P., Papavasileiou, P. & Rajewsky, N. circBase: a database for circular RNAs. *RNA* **20**, 1666–1670 (2014).
47. Pruitt, K. D., Tatusova, T. & Maglott, D. R. NCBI reference sequences (RefSeq): a curated non-redundant sequence database of genomes, transcripts and proteins. *Nucleic Acids Res.* **35**, D61–5 (2007).
48. Fang, S. *et al*. NONCODEV5: a comprehensive annotation database for long non-coding RNAs. *Nucleic Acids Res.* **46**, D308–D314 (2018).
49. Memoli, D. https://identifiers.org/arrayexpress:E-MTAB-15186 (2025).
50. Memoli, D. https://identifiers.org/arrayexpress:E-MTAB-15185 (2025).
51. Memoli, D. https://identifiers.org/arrayexpress:E-MTAB-15369 (2025).

Acknowledgements

This work was supported by AIRC Foundation for Cancer Research, Grant No. IG-23068 (to A.W.), Italian Ministry of University and Research PNRR-MUR NextGenerationEU PRIN 2022, cod. 202282CMEA - CUP: D53D23007790001 (to G.N.) and cod. 2022Y79PT4 – CUP: D53D23008040006 (to A.W.); PNRR-MUR NextGenerationEU PRIN-PNRR 2022 cod. P2022N28FJ - CUP: D53D23016530001 (to G.N.); Italian Ministry of Health (Ricerca Corrente), Young Researcher Grant GR-2021-12373937 (to G.N.) and Grant GR-2018-12366312 (to E.F. and A.W); 5 × 1000 Institutional Grant from CRO Aviano, National Cancer Institute, Istituto di Ricovero e Cura a Carattere Scientifico (IRCCS) seed grant to B.M. and E.F., no grant number provided.

Author contributions

Conceptualization: E.F., G.N., A.S.; investigation: J.L., B.M., D.M., R.G., F.C., A.S., E.F.; bioinformatic analyses: D.M., F.S.; writing and original draft preparation, J.L., G.N., A.S.; writing, review, and editing: J.L., E.F., B.M., G.N., A.S., A.W.; funding acquisition: E.F., B.M., G.N., A.W. All the authors approved the final version of the manuscript.

Competing interests

The authors declare no competing interests.

Additional information

Supplementary information The online version contains supplementary material available at https://doi.org/10.1038/s41597-025-05807-x.

Correspondence and requests for materials should be addressed to A.S., E.F. or G.N.

Reprints and permissions information is available at www.nature.com/reprints.

Publisher's note Springer Nature remains neutral with regard to jurisdictional claims in published maps and institutional affiliations.

Open Access This article is licensed under a Creative Commons Attribution-NonCommercial-NoDerivatives 4.0 International License, which permits any non-commercial use, sharing, distribution and reproduction in any medium or format, as long as you give appropriate credit to the original author(s) and the source, provide a link to the Creative Commons licence, and indicate if you modified the licensed material. You do not have permission under this licence to share adapted material derived from this article or parts of it. The images or other third party material in this article are included in the article's Creative Commons licence, unless indicated otherwise in a credit line to the material. If material is not included in the article's Creative Commons licence and your intended use is not permitted by statutory regulation or exceeds the permitted use, you will need to obtain permission directly from the copyright holder. To view a copy of this licence, visit http://creativecommons.org/licenses/by-nc-nd/4.0/.

© The Author(s) 2025